Journal of King Saud University – Computer and Information Sciences (2015) 27, 334–343

King Saud University

Journal of King Saud University – Computer and Information Sciences

www.ksu.edu.sa
www.sciencedirect.com

Source localization algorithms to find attention and memory circuits in the brain

M. Sabeti [a,*], S.D. Katebi [b], K. Rastgar [c]

[a] Department of Computer Engineering, College of Engineering, Shiraz Branch, Islamic Azad University, Shiraz, Iran
[b] Department of Computer Engineering, College of Engineering, Zarghan Branch, Islamic Azad University, Zarghan, Iran
[c] Department of Physiology, Shiraz University of Medical Sciences, Shiraz, Iran

Received 29 December 2013; revised 23 October 2014; accepted 9 December 2014
Available online 25 June 2015

KEYWORDS

P300 event-related potential;
EEG source localization

Abstract Brain is a complex organ and many attempts have been done to know its functions. Studying attention and memory circuits can help to achieve much information about the brain. P300 is related to attention and memory operations, so its investigation will lead to better understanding of these mechanisms. In this study, EEG signals of thirty healthy subjects are analyzed. Each subject participates in three-segment experiment including start, penalty and last segments. Each segment contains the same number of visual and auditory tests including warning, attention, response and feedback phases. Data analysis is done by using conventional averaging techniques and P300 source localization is carried out with two localization algorithms including low-resolution and high-resolution algorithms. Using realistic head model to improve the accuracy of localization, our results demonstrate that the P300 component arises from a wide cerebral cortex network and localizing a definite generating cortical zone is impossible. This study shows that a combination of high-resolution and low-resolution algorithms can be a useful tool for physiologists to find the neural sources of primary circuits in the brain.

1. Introduction

Contribution of the brain neural circuitry to cognitive processes is one of the main aspects of neuroscience which is so difficult in practice, and many attempts have been made to describe the function of the brain. Electroencephalogram (EEG) (Nunez and Srinivasan, 2006; Sanei and Chambers, 2007) signals are produced by recording brain electrical activity through scalp electrodes and because of convenience and low cost they still have a remarkable value in brain activity monitoring (Parvinnia et al., 2014).

Event Related Potentials (ERPs) (Polich, 2007; Luck, 2005) reflect the brain electrical responses to different sensory, cognitive or affective stimuli. Compared to functional magnetic resonance imaging (fMRI) and positron emission tomography (PET), ERPs have better temporal resolution but less definite

* Corresponding author.
E-mail address: sabeti@iaushiraz.ac.ir (M. Sabeti).
Peer review under responsibility of King Saud University.

Production and hosting by Elsevier

http://dx.doi.org/10.1016/j.jksuci.2014.12.002
1319-1578

spatial resolution. By increasing the number of scalp electrodes theoretically we can improve their spatial resolution. However, it should be considered that when the number of scalp electrodes is increased, the inter-distances between electrodes are decreased (or the cross-talk among them is increased). The most well-known component of ERPs is the P300 which is in close relationship with memory/attention activities of the brain. Using depth electrodes in medial temporal regions in epileptic patients, the hippocampal formation was demonstrated as the source of P300 for the first time (McCarthy et al., 1989). But other studies on patients that had temporal lobectomy or severe medial temporal lobe injury showed that the hippocampal formation cannot be the exclusive source of this wave (Molnar, 1994). An interaction between frontal lobe and hippocampal/temporal parietal region was known as the generator of P300 (Knight, 1997; Kirino et al., 2000). Involvement of frontal, parietal, temporal and cingulate areas as the P300 source was confirmed with fMRI studies (Stevens et al., 2000).

Many algorithms have been made for reconstructing the current source for a given scalp electrical distribution. Source localization based on scalp potentials requires a solution to an ill-posed inverse problem with many possible solutions. A good understanding of brain physiology is critical for selection of a particular solution (Sanei and Chambers, 2007). EEG source localization methods can be categorized into two main approaches: equivalent current dipole approach, in which the EEG signals are assumed to be generated by a relatively small number of focal sources, and the current distributed source approach, in which all possible source locations are considered simultaneously.

The distributed source approach has good consistency with neuroimaging studies, so it could be significantly useful in determining the underlying sources of P300. Among this approach, localization algorithms such as low resolution electromagnetic tomography (LORETA) (Sabeti et al., 2011; Pascual-Marqui et al., 1994), standardized LORETA (sLORETA) (Pascual-Marqui, 2002), focal underdetermined system solver (FOCUSS) (Gorodnitsky et al., 1995) and shrinking LORETA-FOCUSS (Liu et al., 2005) have been proposed.

Mulert et al. (2004) used LORETA in the analysis of P300 data and found a large similarity between the result of LORETA and previous fMRI or intracranial recordings studies. Volpe et al. (2007) applied LORETA to analyze the two P300 sub-components (P3a and P3b) and found that P3a is related to the automatic allocation of attention, while P3b reflects the effortful processing of task-relevant events. Schimpf and Liu (2008) used SSLOFO to localize the P300 ERP neural generators. They showed that the results are in line with functional neuroimaging studies while preserving the temporal resolution advantages of the EEG.

Li et al. (2009) applied EEG/fMRI integration to investigate the neural sources of P300 component. Their results revealed that P300 was generated in a distributed network such as bilateral parietal, middle and inferior frontal, precentral, postcenteral cortex and anterior cingulate gyrus. Connell et al. (in press) studied neural sources of P3a and P3b components with simultaneous EEG/fMRI recordings for visual oddball task and showed that the effect of age on P3a component was increased activation of the left inferior frontal and cingulate cortex and decreased activation of the inferior parietal cortex. This effect on P3b was the increased activation of the left temporal regions, right hippocampus, and right prefrontal cortex.

In this study, visual and auditory paradigms are used to record P300 ERP in a group of healthy participants. Whereas the neural sources of P300 component are not determined certainly, localization of brain sources of this component is the main goal of this work. In our study, sLORETA and shrinking sLORETA are used to localize the cortical distribution of P300 generators. To improve the accuracy of localization, we used the realistic head model instead of spherical model to estimate the lead-field matrix. Also, we restricted source space (solution space) to parts of the brain that believed they are related to attention and memory circuits. Finally, the results are compared and discussed.

The paper is organized as follows. Section 2 will discuss data collection. In Section 3, we present EEG source localization algorithms. Experimental results that show the neural sources of P300 component, are introduced in Section 4. Finally, Sections 5 and 6 summarize the contribution of this paper and some future research directions respectively.

2. Data collection

Thirty normal subjects (20 male and 10 female) aged between 18 and 30 years (23.10 ± 3.84 year) participated in this study. All participants were students and they were recruited from Shiraz University, Shiraz, Iran. Each participant has been seated upright with eyes open and the experiment lasted around 150 min. To avoid any muscle artifact the neck was firmly supported by the back of the chair, and the feet were rested on a footstep.

Each subject participated in three-segment experiments including start (takes about 30 min), penalty (60–90 min) and last (30 min) segments. Each segment contains an equal number of visual and auditory tests where each test includes warning, attention, response and feedback phases. Fig. 1 shows a simple illustration of the visual test. At the beginning of each test, the participant sees two up and down flashes, as an alarm. In the attention phase, one of the flashes appears. In the response phase, a question mark appears and the participant must answer which flash has appeared by pressing up or down button. In the feedback phase, a right/wrong answer is displayed. The auditory test is similar, in structure, to the visual test, but the participant distinguishes between low or high pitch tones from the background white noise. The visual and auditory tests are applied alternatively, and to start the next test, participants must press a button. Each visual or auditory test lasts about 7 s. In this work, each segment contains one hundred visual tests and one hundred auditory tests. In penalty

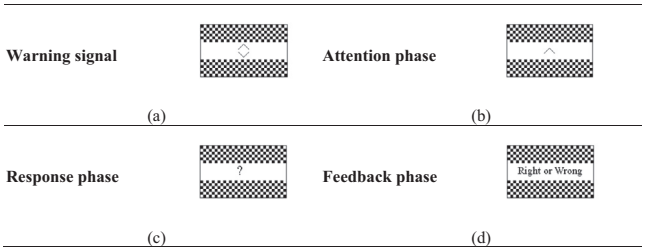

Figure 1 Illustration of visual experiment.

segment, we punish participants for wrong answers where each wrong answer adds four more tests to this segment. Therefore, the penalty segment takes a long time in comparison to the other segments.

Electrophysiological data were recorded using a neuroscan 32 channel Synamps system, with a signal gain equal to 75 K (150x at the headbox). For EEG paradigms, 30 electrodes (Electrocap 10–20 standard system with reference to linked earlobes) were recorded plus vertical electrooculogram (VEOG). The eye-blink artifacts were corrected using the Infomax independent component analysis (ICA) algorithm (Bell and Sejnowski, 1995) and the elimination of high noise trials were performed off-line by an experienced physician through visual inspections of the recordings (Sabeti et al., 2009). Additionally, EEG signals were filtered with a band pass filter at 0.5–45 Hz to account for noise of very low frequency up to the power line frequency. According to the international 10–20 system, EEG data have been continuously recorded from 30 electrodes (Fp1, Fp2, F3, F4, FC3, FC4, C3, C4, CP3, CP4, P3, P4, O1, O2, F7, F8, FT7, FT8, T3, T4, TP7, TP8, T5, T6, Fz, FCz, Cz, CPz, Pz, Oz) with a sampling frequency of 250 Hz.

3. EEG source localization

The EEG signal can be described by the propagation of the brain sources to the sensors with the assumption that a small region of active tissue in the brain can be represented by current dipole source

$$X = LS + N = \sum_{i=1}^{m} L_i s_i + N \tag{1}$$

where X (an $n_e \times T$ matrix) represents the EEG channel data, S (an $m \times T$ matrix) is the current source densities, N is noise and Lead field matrix, L, is an $n_e \times m$ matrix describing the forward mixing model of m sources to the n_e electrodes. The lead field matrix, L, can be decomposed into m matrices L_i as

$$L = [L_1 \cdots L_i \cdots L_m] \tag{2}$$

where L_i is an $n_e \times 1$ vector containing the potentials observed at the electrodes when the source vector has unit amplitude at one location and is zero at all others. This matrix contains the geometric information about the source and sensor positions, as well as the volume-conductor properties. Fig. 2 shows the used scheme for P300 source localization.

3.1. Head model

Most previous studies assume that the head model is made up of a set of nested concentric spheres (including scalp, skull, and brain) each with homogeneous (same magnitude at all locations) and isotropic (same magnitude in all directions) conductivity. However, it is clear that the head is not spherical, so replacing the spherical geometry with a more realistic head shape improves the lead-field matrix calculations. This realistic head model can be extracted from MRI anatomical images. This model assumes that the head consists of a set of contiguous isotropic regions with constant conductivity. Table 1 shows the radius and conductivity of different head tissues. The radius of each tissue is selected by fitting a sphere to the template MRI image. As Table 1 shows the skull is the most important tissue because of its low conductivity where the brain to skull conductivity ratio is usually considered as 80.

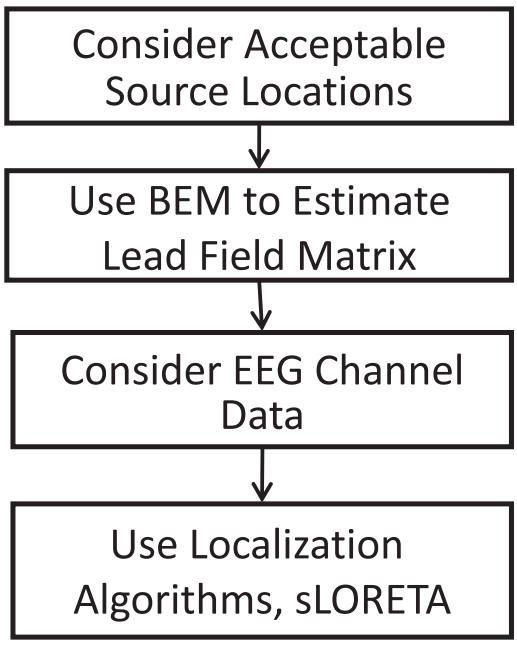

Figure 2 Source localization scheme.

Table 1 Tissue conductivity.

Tissue	Radius (mm)	Conductivity $1/(\text{ohm} \cdot \text{mm})$
Brain	75.2479	0.3300
Skull	81.9291	0.0041
Scalp	96.2195	0.3300

3.2. Boundary element model

To calculate the lead field matrix, it must be investigated how currents spread through the brain, skull and scalp. In fact, elements of lead field matrix show the surface potentials generated by the neural sources in the brain. It is clear that the surface potentials depend on realistic shape and conductivity information. Since an analytic solution for surface potentials is available only for simple surfaces, use of realistic volume requires numerical techniques such as the boundary element model (BEM) (Fuchs et al., 1998). This method gives a solution by calculating the effects of the source at the boundaries of the volume where the boundaries are the interfaces between regions of different conductivities within the volume and the outer surface.

It is assumed that the volume can be divided into $n_S + 1$ regions with conductivities $\sigma_j,\ j = 1, \ldots,\ n_S + 1$, which includes the nonconducting region outside of the head. These regions are separated by a number of n_S surfaces S_j with different conductivities σ_j. Using Green's theorem for solving Poisson equation ($\sigma \cdot \nabla^2 V = \nabla J^i$), the potential at any point consists of the sum of an infinite medium potential $v_\infty(r)$ and the volume current effects, as

$$\frac{\sigma_k^- + \sigma_k^+}{2} v(r) = \sigma_0 v_\infty(r) + \frac{1}{4\pi} \sum_{j=1}^{ns} (\sigma_j^- - \sigma_j^+) \cdot \int_{S_j} v(r') \nabla \left(\frac{1}{r' - r} \right) \cdot dr' \tag{3}$$

$$v_\infty(r) = \frac{1}{4\pi\sigma_0} \int_G j^i(r') \cdot \nabla \left(\frac{1}{r' - r} \right) dr' \tag{4}$$

where $v_\infty(r)$ shows the potential generated by the impressed current density, J^i in an infinite homogeneous medium with conductivity σ_0, $r' - r$ is the vector distance from an arbitrary point r to the element of volume or area r', and σ_j^- (σ_j^+) indicates the conductivity inside (outside) the j th surface respectively. Eqs. (3) and (4) form the general set of boundary integral equations for solving the forward problem for scalp potentials (calculating the lead field matrix). To calculate the electric fields it is necessary to numerically approximate the integral over the closed surfaces S_j of the conductor boundaries. The surfaces can be described by a large number of small triangles and the integrals are replaced by summations over these triangle's areas. These small triangles can be obtained from segmentation of the MRI anatomical data and triangulation of the corresponding surfaces. The brain template used is obtained from Montreal Neurological Institute (MNI) that is an averaged T1-weighted MR scan from 152 subjects (Neurological Institute and Hospital), (Spm8 (statistical parametric mapping)). The assumed head model contains three layers: brain, skull and scalp. Each surface is decomposed into 5120 small triangles (2562 vertices). Fig. 3 shows the adopted head model.

3.3. Source locations

In this study, we include the anatomical information by only considering the locations corresponding to physically realistic source locations. We restricted the source space (solution space) to parts of the brain that are believed to be related to attention and memory circuits. This method limits the solution space, therefore it can improve the accuracy of localization. The probable source locations are shown in Fig. 4. This figure contains the brain cortex and limbic system where physiologists believe that attention and memory circuits are located in. These locations register to Talairach human brain atlas (Wong), (Talairach and Tournoux, 1988) and are obtained from MNI brain template.

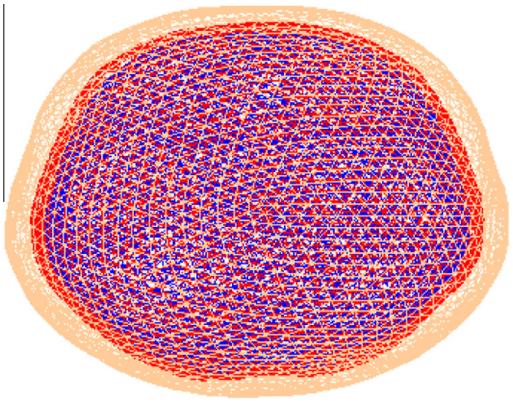

Figure 3 Assumed head model including three layers: brain, skull and scalp.

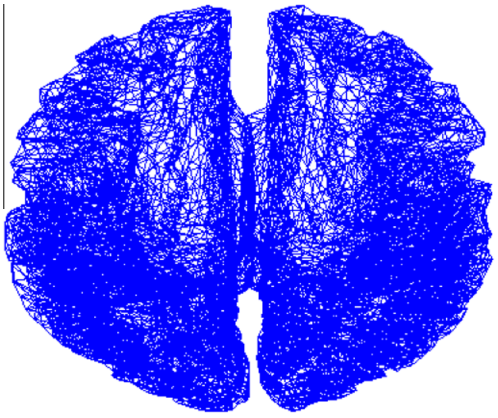

Figure 4 Source locations including the cortex and limbic system.

3.4. Source localization algorithm

The goal of source localization is to find the intracerebral sources of the potentials recorded at the scalp and to relate them to the activity of neural generators within the brain. Source localization based on scalp potentials requires a solution to an ill-posed inverse problem with many possible solutions. Selection of a particular solution often requires a priori knowledge from the overall physiology of the brain. It is important to utilize methods that help the physiologist to perform the essential operation of transferring scalp EEG information into cortical or even subcortical processes. Also the selected methods should be easily interpreted by specialists.

First localization algorithm, sLORETA (Pascual-Marqui, 2002) gives a unique solution to the inverse problem using a cost function as

$$||X - LS||^2 + \lambda ||S||^2 \tag{5}$$

where λ is a positive constant known as the regularization parameter and $||.||$ is the Euclidean norm. Hence sLORETA chooses S to fit EEG channel data X in least-squares sense, but penalizes solutions of large norm. sLORETA gives a solution as

$$s_i = L_i^T [L_i L_i^T + \lambda_i I]^{-1} X \tag{6}$$

Second localization algorithm, shrinking sLORETA (Liu et al., 2005) assumes that sources are more focal, and produces a high spatial resolution iterative method that uses information from the previous iterations. In this algorithm, the search space is modified by eliminating the nodes with no source activities. In fact, this algorithm shrinks the source space after each iteration, leading to a reduction in computational cost. Table 2 shows the shrinking sLORETA source localization algorithm.

To obtain the temporal information, the sources are assumed spatially fixed during a short time window, and temporal information can be factored out (Sanei and Chambers, 2007; Liu et al., 2005). The solution of each time sample is added to obtain temporal information as

$$S = \sum_t \hat{S}_t, \tag{7}$$

$$\hat{S}_t = SS^T L^T (LSS^T L^T)^+ X \tag{8}$$

where $\hat{S}_t$ is calculated by sLORETA and shrinking sLORETA.

Table 2 The shrinking sLORETA source localization algorithm.

1. Estimate the current density $\hat{S}_0$ by sLORETA spatial filter
2. Initialize the weighting matrix C as
   $C_0 = (W_0^{-1})^T W_0^{-1}$
   $W_0 = diag(\hat{S}_0(1), \hat{S}_0(2), ..., \hat{S}_0(3m))$
3. Estimate the source power as
   $\hat{S}_i^T(l)[L_i(l,l)]^{-1}\hat{S}_i(l)$
4. Keep the prominent nodes and their neighboring nodes, and smooth the values on these nodes
5. Shrink the solution space containing only the retained nodes
6. Update the weighting matrix as
   $W_i = PW_{i-1}[diag(\hat{S}_{i-1}(1), \hat{S}_{i-1}(2), ..., \hat{S}_{i-1}(3m))]$
   $P = diag\left[\frac{1}{\|K_1\|} ... \frac{1}{\|K_{3m}\|}\right]$
7. Repeat steps 3 to 6 until there is no negligible change in the weighting matrix

4. Experimental results

In this study, we try to localize P300 component in the start segment using sLORETA and shrinking sLORETA localization algorithms. These algorithms estimate activity in different source locations by solving $X = LS$. In these algorithms, the goal is estimation of S where X and L is defined. The elements of X matrix show the EEG brain activity in electrodes located on the head based on 10–20 standard system.

In the next step, to calculated elements of L matrix, the possible source locations must be determined. Whereas the brain is not spherical, it should be better that source locations are considered according to the real shape of the brain. Also as physiologists discuss (Bear et al., 2006), all parts of the brain are not known as P300 generator and only some specific areas are responsible for its generation, so we limited source locations to the specific areas of the brain like the cortex and limbic system.

Finally, L matrix will be calculated. To calculate the first column of L ($n_e \times m$ matrix), we assume that the first source in location (x_1, y_1, z_1) is active. Using a numerical method (BEM), first the voltage on the cortex will be calculated. At the next steps, the voltage on the skull and scalp will be calculated respectively. In fact, each column of L contains the potentials observed at the electrodes when the source vector has unit amplitude at one location and the other sources are all zero. After determining L matrix, two mentioned localization algorithms will be applied to find the neural sources of P300 component with estimating of S matrix elements.

Whereas, the neural sources of P300 were not determined certainly, we cannot estimate localization error for P300 sources. Therefore, to evaluate the accuracy of localization algorithms, we used simulated data.

4.1. Simulated data

To evaluate the source localization algorithms, we consider sinusoidal sources in a simulated brain. Two sources with a 1 μV amplitude, oscillating sinusoidally at 23 Hz are considered. These sources are randomly positioned in the brain and gaussian white noise is added to yield a signal to noise ratio (SNR) of 2. Fig. 5 and Fig. 6 show the result of applying sLORETA and shrinking sLORETA using spherical and realistic head model respectively. Fig. 5a shows that the output of sLORETA is a blurred image of neural activity in the brain and it is difficult to accurately locate the position of the sources. Fig. 5b shows that using shrinking sLORETA, there are localization errors E_{loc} = 5.34 mm and E_{loc} = 75.23 mm for the superficial and deeper sources respectively. Fig. 6a shows that sLORETA can detect only the superficial source correctly. Fig. 6b shows that the shrinking sLORETA can detect the superficial source correctly, but there is a localization error E_{loc} = 6.80 mm for the deeper source. Our results show that the accuracy of source localization is improved using the realistic head model.

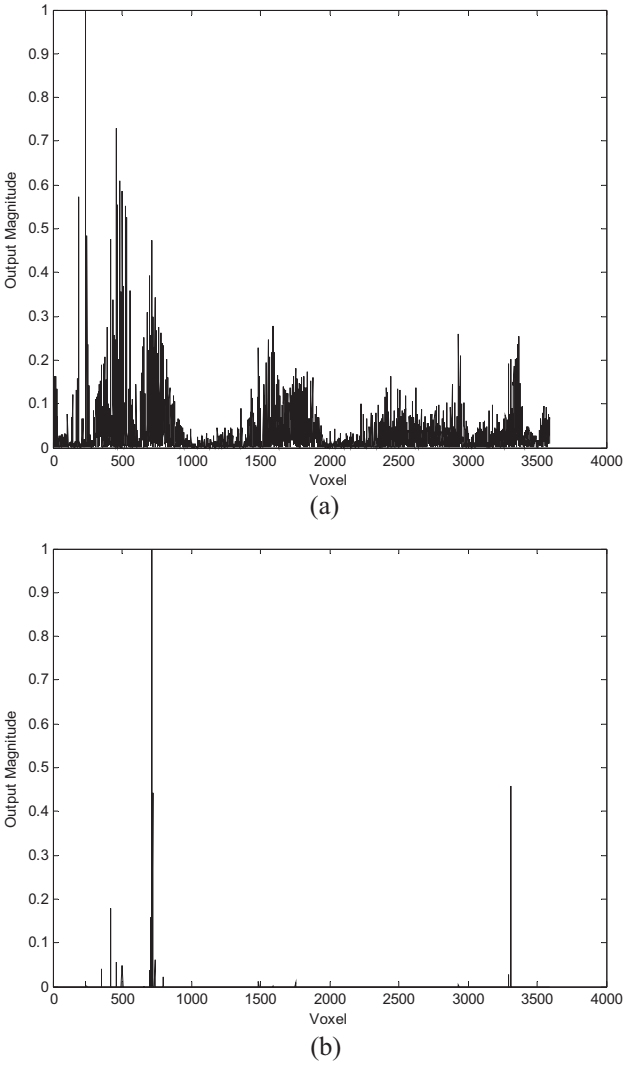

Figure 5 Activation map of source power with spherical head model using (a) sLORETA, (b) shrinking sLORETA.

4.2. P300 source localization

Because ERP is embedded in a larger EEG signal, almost all ERP studies rely on some sort of averaging procedure to minimize the EEG noise. The advantage of averaging event-related data is not only to enhance the signal, but also to remove non-event-related noise. EEG epochs following a given stimulus are extracted from the ongoing EEG. The ERP is obtained by

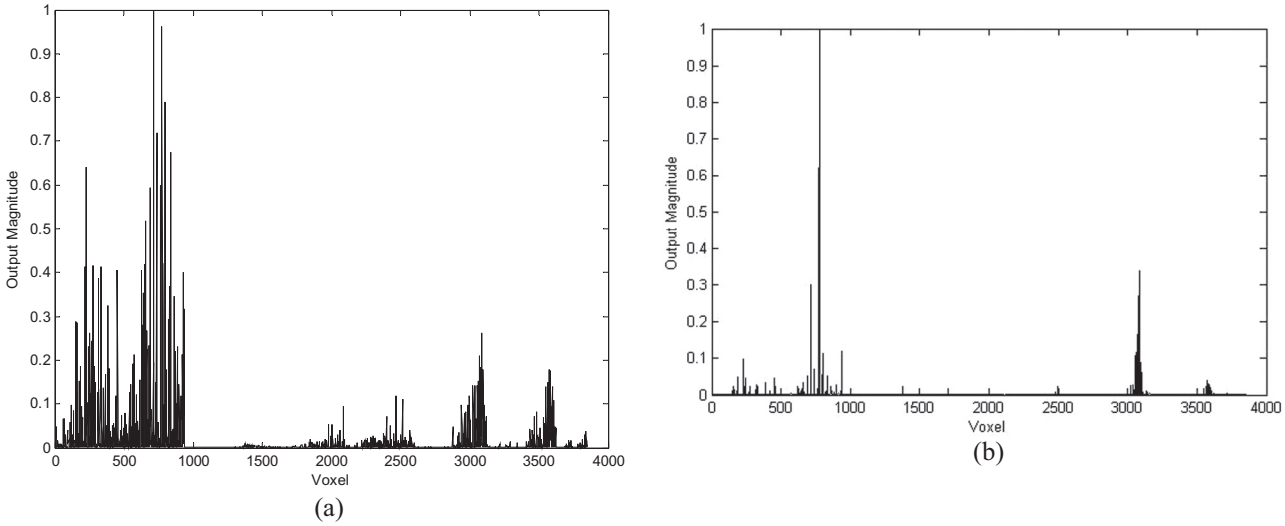

Figure 6 Activation map of source power with realistic head model using (a) sLORETA, (b) shrinking sLORETA.

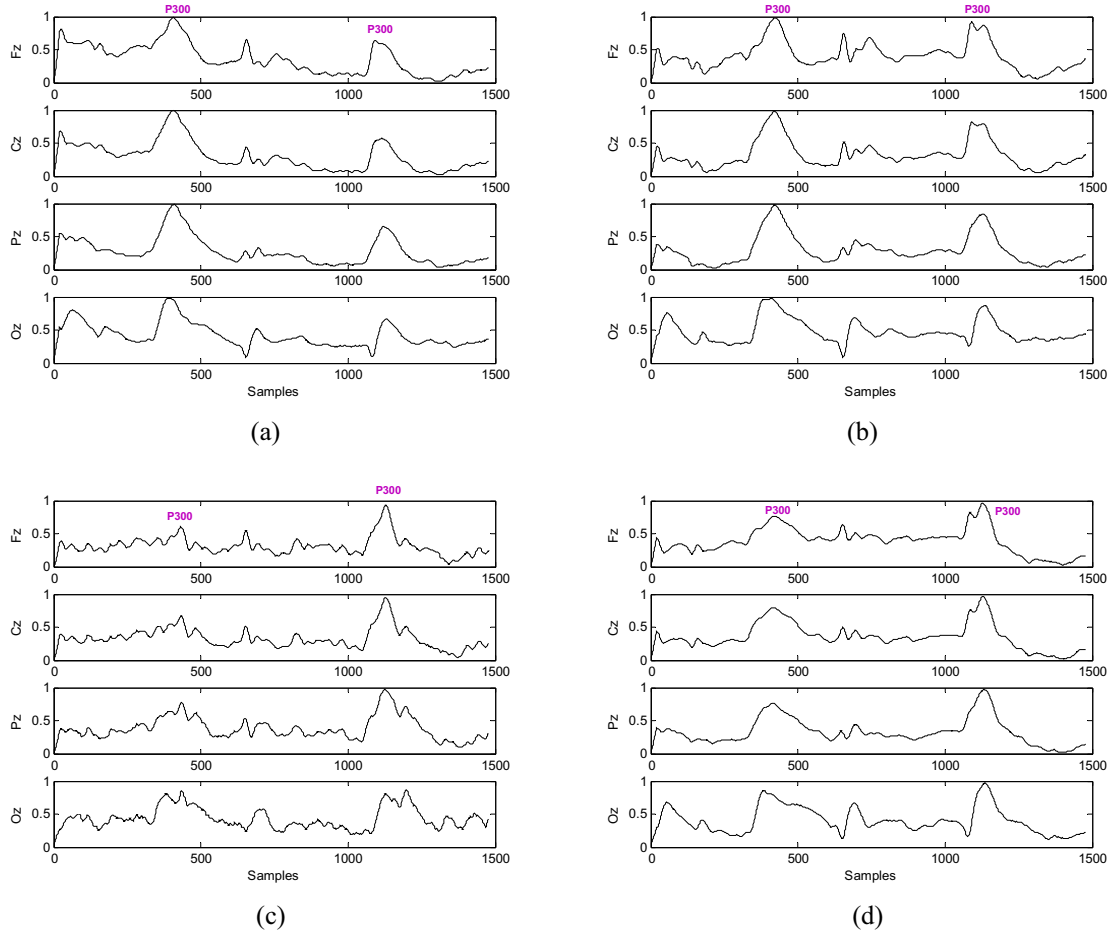

Figure 7 Grand averaging process of all subjects on the Fz, Cz, Pz, Oz channels on the visual task in (a) the first segment,(b) right answer, (c) wrong answer in the penalty segment, (d) the last segment.

temporally averaging event-related data (more than 40 events), each event producing an EEG of size $n_e \times T$, where n_e is the number of electrode signals and T is the number of samples of the event. Figs. 7 and 8 show the grand averaging process of all subjects on Fz, Cz, Pz and Oz channels for start, penalty and last phase. In this study, attention and feedback phase in both visual and auditory experiments elicited the P300 component. With change of stimulus discrimination (harden the experiment) during the experiment, we ensured that the number of correct answers remains above a certain threshold.

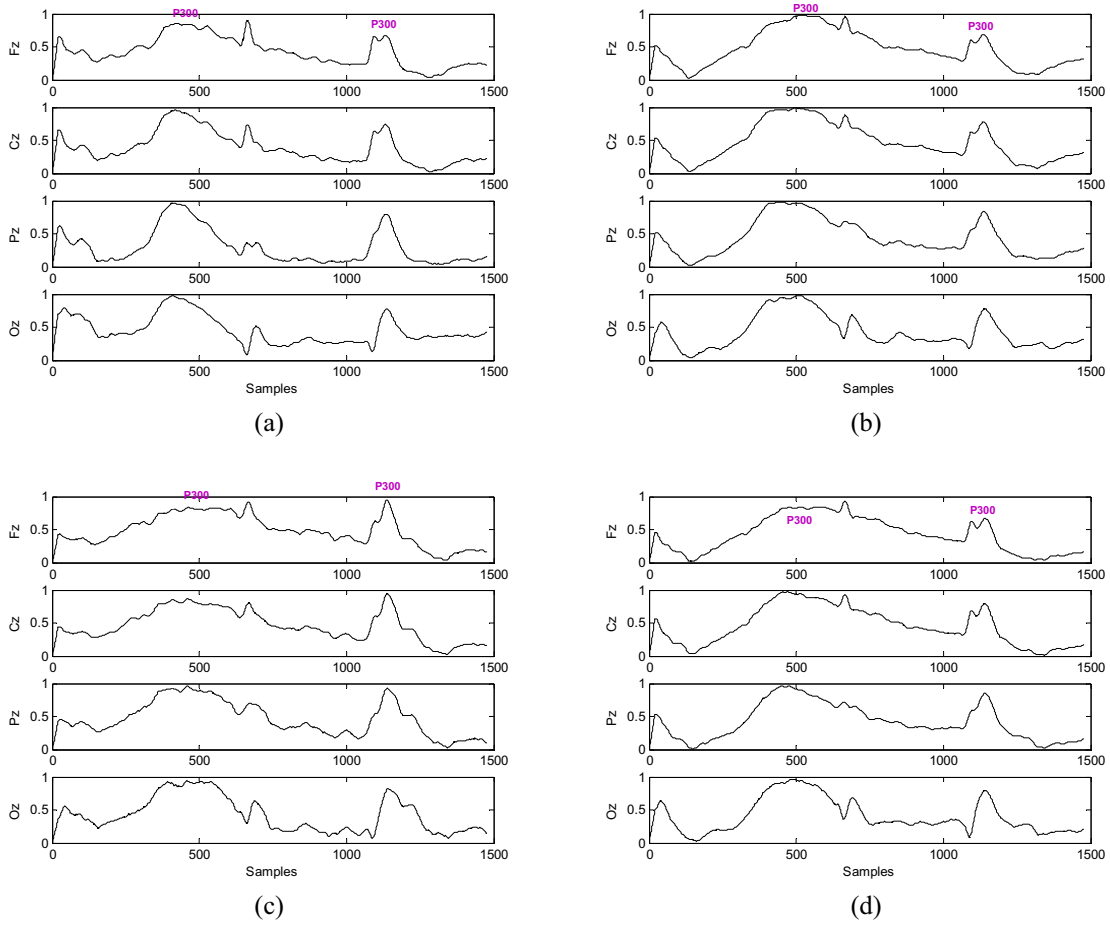

Figure 8 Grand averaging process of all subjects on the Fz, Cz, Pz, Oz channels on the auditory task in (a) the first segment,(b) right answer, (c) wrong answer in the penalty segment, (d) the last segment.

Table 3 Mean and std of latency for P300 component in the first and last segments.

	First segment	Last segment
Visual stimuli	357.6915 ± 4.7522	361.7711 ± 9.6603
Auditory stimuli	366.3483 ± 8.1565	398.7662 ± 20.5237

Table 4 Mean and std of latency for P300 component in the penalty segments.

	Right answer	Wrong answer
Visual stimuli	369.3134 ± 2.5310	377.3930 ± 1.7156
Auditory stimuli	413.2338 ± 1.4547	392.0000 ± 4.7103

Figs. 7 and 8 show that the more the attention to environmental feedback, the higher is the P300 peak. In the penalty phase the feedback P300 peak for wrong answer is increased because of more attention and higher tension.

Tables 3 and 4 show the mean and the standard deviation of latency for P300 component in the first, penalty and last segments. It is shown that the P300 latency is longer for auditory stimuli compared to visual stimuli (p-value < 0.05). The reason might be that the auditory test is more difficult than the visual test, and our results confirm that the number of auditory correct answers is lower than that for visual test. Table 5 shows the probability of correct and incorrect answers for the two stimulus types. We compared the latency of P300 component for first and last segments. Latency of P300 component is increased in the last segment compared to the first due to participants' fatigue (p-value < 0.05).

Table 5 Probability of correct and incorrect answers.

Type of test	Probability of correct answer (mean ± std)
Visual test	89.12 ± 8.72
Auditory test	88.28 ± 12.87

We localized P300 component in the start segment. The neural generators of the P300 component are analyzed for a grand averaging of all subjects using sLORETA and shrinking sLORETA algorithms. Fig. 9 shows the result of applying sLORETA to the ERP data. It is clear that the source distribution generated by sLORETA has a low spatial resolution. The output of sLORETA is a blurred image of neural activity in the brain which makes it difficult to accurately locate the position of the sources. Therefore, a higher spatial resolution algorithm also is needed.

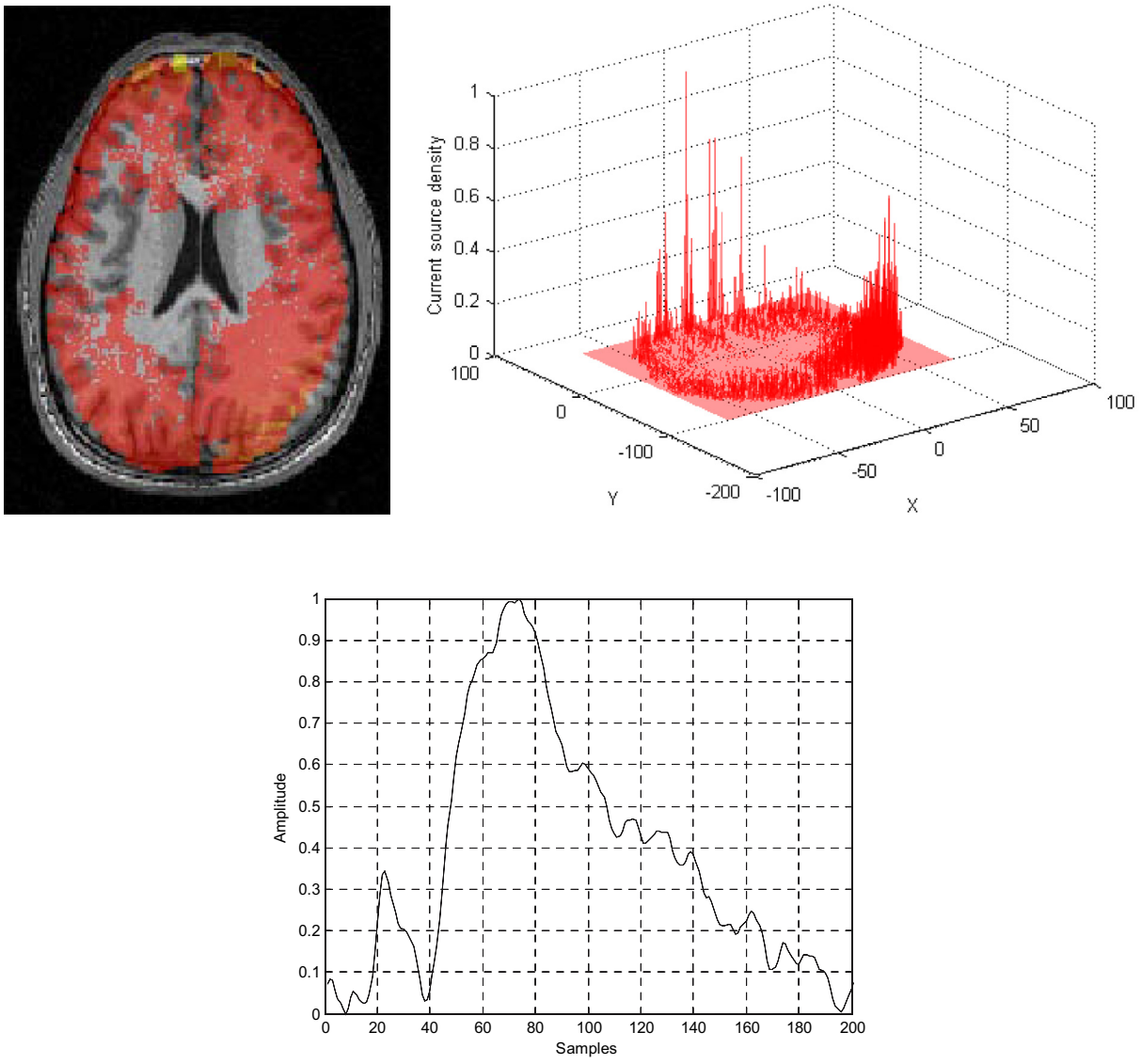

Figure 9 Reconstructed activation map of signal power, and reconstructed P300 waveform using the sLORETA.

Fig. 10 and Table 6 show the result of applying shrinking sLORETA to the ERP data. A high-resolution method such as shrinking sLORETA is able to localize more focal sources, but this method is not generally robust for distributed activity and may generate over-focal results. Therefore high-resolution is not necessarily better than low-resolution algorithms. It should be emphasized that both low and high resolution have their own appropriate applications.

5. Discussion

P300 is believed to have relation with attention and memory operation and possibly arises from a distributed network of neurons. Determining a distinct explanation for this phenomenon is so difficult. P300 is generated whenever a task requires stimulus discrimination, that is occurred in many aspects of cognition specially attention (Polich, 2007).

In our study, sLORETA showed that the P300 is generated in a wide cerebral network including the superior and inferior frontal lobe, middle temporal gyrus, parietal lobe, and cingulate gyrus. Shrinking sLORETA showed that the P300 generated by superior and inferior frontal lobe and cingulate gyrus. There are no significant differences between the patterns of activation for two stimulus types. Our results for the source activity underlying a target detection task are in line with those reported in recent studies that the P300 wave is generated by numerous circuits in the brain responsible for working memory and attention. Although several studies (Li et al., 2009; Connell et al., in press) used fMRI to localize P300 neural sources, but EEG signal remains a useful tool to monitor the brain activity. The main advantage of EEG in comparison with fMRI is low cost and easy usability.

Using realistic head model to improve the accuracy of localization, our results demonstrate that some parts of P300 component originate from the interaction between frontal lobe and temporal–parietal areas, and other parts of P300 are generated by the cingulate gyrus that has a significant role in working memory circuit. In an attempt to find a specific source for P300 generation, we cannot find a specific area of the brain

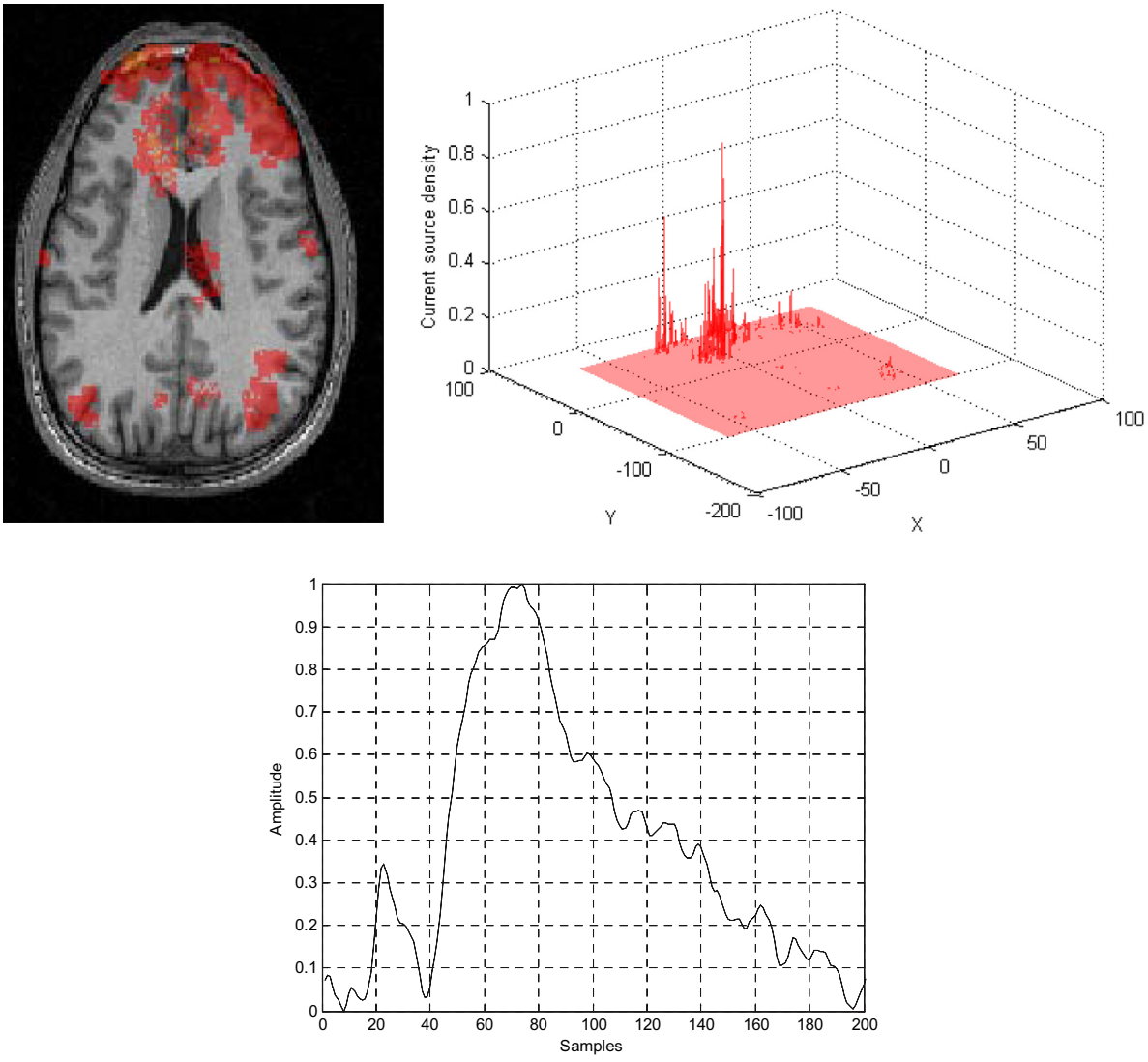

Figure 10 Reconstructed activation map of signal power, and reconstructed P300 waveform using the shrinking sLORETA.

Table 6 Cerebral networks found by shrinking sLORETA.

MNI coordinates			Brodmann area	
X	*Y*	*Z*		
−4.9523	23.8364	56.6187	Brodmann area 8	Superior Frontal Gyrus Frontal Lobe
−19.1222	62.2029	2.4246	Brodmann area 10	Superior Frontal Gyrus Frontal Lobe
8.0032	37.2007	−19.8804	Brodmann area 11	Inferior Frontal Gyrus Frontal Lobe
16.3513	64.0694	16.4875	Brodmann area 10	Superior Frontal Gyrus Frontal Lobe
−7.6598	19.7742	47.2293	Brodmann area 32	Cingulate Gyrus Limbic Lobe

responsible for generating P300. This result confirms previous studies with different experimental techniques that the P300 stems from a diffuse neuronal network in the brain (Brazdil et al., 2005; Linden, 2005).

sLORETA and shrinking sLORETA localization algorithms have been selected because they assume that any source can be considered as a weighted combination of dipoles (Mosher et al., 1999). So, the geometry of sources can be distributed instead of being localized. Furthermore, these algorithms do not require determination of the number of dipole sources to fit to the data. Therefore, the anatomical information can be easily included by only considering the locations

corresponding to physically realistic source locations. Physiologists (Bear et al., 2006) believe that attention and memory circuits are located in the cortex and the limbic system. Therefore, we restricted the source space to probable P300 generating areas of the brain.

6. Conclusion

It is clear that the head is not spherical, so replacing the spherical geometry with a more realistic head shape improves the lead-field matrix calculations, and finally enhances the accuracy of source localization algorithms. Also, we include the anatomical information by only considering the locations corresponding to physically realistic source locations. We restrict the source space to parts of the brain that are believed to be related to attention and memory circuits. This method limits the solution space, therefore it can improve the accuracy of localization.

The high-resolution method such as shrinking sLORETA is able to localize more focal sources, but these methods are not generally robust to distributed activity and may generate over-focal results. Therefore high-resolution is not necessarily better than low-resolution algorithms. It should be emphasized that both low and high resolution have their own appropriate applications, so it seems that physiologists need both low and high-resolution results. This study shows that a combination of high-resolution and low-resolution algorithms can be a useful tool for physiologists to find the neural sources of primary circuits in the brain. We studied P300 sources only in start segment. Analyzing P300 sources in penalty and last phases is planned as a future work. We decide to study how P300 neural sources are affected by penalty and fatigue.

References

Bear, M.F., Connors, B.W., Paradiso, M.A., 2006. Neuroscience: Exploring the Brain. Lippincott Williams and Wilkins.

Bell, A.J., Sejnowski, T.J., 1995. An information-maximization approach to blind separation and blind deconvolution. Neural Comput. 7, 1129–1159.

Brazdil, M., Dobsik, M., Mikl, M., Hlustik, P., Daniel, P., Pazourkova, M., Krupa, P., Rektor, I., 2005. Combined event-related fMRI and intracerebral ERP study of an auditory oddball task. Neuroimage 26, 285–293.

Connell, R.G., Balsters, J.H., Kilcullen, S.M., Campbell, W., Bokde, A.W., Lai, R., Upton, N., Robertson, I.H., 2012. A Simultaneous ERP/fMRI Investigation of the P300 Aging Effect. Neurobiol. Aging 33 (10), 2448–2461.

Fuchs, M., Drenckhahn, R., Wischmann, H.A., Wagner, M., 1998. An improved boundary element method for realistic volume-conductor modeling. IEEE Transact. Biomed. Eng. 45 (8), 980–997.

Gorodnitsky, I.F., George, J.S., Rao, B.D., 1995. Neuromagnetic source imaging with FOCUSS: a recursive weighted minimum norm algorithm. Electroencephalogr. Clin. Neurophysiol. 95, 231–251.

Kirino, E., Belger, A., Goldman-Rakic, P., McCarthy, G., 2000. Prefrontal activation evoked by infrequent target and novel stimuli in a visual target detection task: an event-related functional magnetic resonance study. J. Neurosci. 20, 6612–6618.

Knight, R.T., 1997. Distributed cortical network for visual attention. J. Cogn. Neurosci. 9, 75–91.

Li, Y., Wang, L.Q., Hu, Y., 2009. Localizing P300 generators in high-density event-related potential with fMRI. Med. Sci. Monit. 15 (3), 47–53.

Linden, D.E., 2005. The P300: where in the brain is it produced and what does it tell us? Neuroscientist 11, 563–576.

Liu, H., Schimpf, P.H., Dong, G., Gao, X., Yang, F., Gao, S., 2005. Standardized shrinking LORETA-FOCUSS (SSLOFO): a new algorithm for spatio-temporal EEG source reconstruction. IEEE Transact. Biomed. Eng. 52 (10), 1681–1691.

Luck S.J., 2005. An Introduction to the Event-Related Potential Technique. The MIT Press. References and further reading may be available for this article. To view references and further reading you must purchase this article.

McCarthy, G., Wood, C.C., Williamson, P.D., Spencer, D., 1989. Task-dependent field potentials in human hippocampal formation. J. Neurosci. 9, 4235–4268.

Molnar, M., 1994. On the origin of the P300 event-related potential component. Int. J. Psychophysiol. 17, 129–144.

Mosher, J.C., Leahy, R.M., Lewis, P.S., 1999. EEG and MEG: forward solutions for inverse methods. IEEE Transact. Biomed. Eng. 46 (3), 245–259.

Mulert, C., Pogarell, O., Juckel, G., Rujescu, D., Giegling, I., Rupp, D., Mavrogiorgou, P., Bussfeld, P., Gallinat, J., Moller, H.J., Heger, U., 2004. The neural basis of the P300 potential. Eur. Arch. Psychiatry Clin. Neurosci. 254, 190–198.

Montreal Neurological Institute and Hospital, McGill University, Canada.

Nunez, P.L., Srinivasan, R., 2006. Electric Fields of the Brain: The Neurophysics of EEG. Oxford University Press, New York.

Parvinnia, E., Sabeti, M., Zolghadri, M., Boostani, R., 2014. Classification of EEG signals using adaptive weighted distance nearest neighbor algorithm. J. King Saud Univ. – Comput. Inf. Sci. 26 (1), 1–6.

Pascual-Marqui, R.D., 2002. Standardized low-resolution brain electromagnetic tomography: technical details. Methods Findings Exp. Clin. Pharmacol. 24(D): 5–12.

Pascual-Marqui, R.D., Michel, C.M., Lehmann, D., 1994. Low resolution electromagnetic tomography: a new method for localizing electrical activity in the brain. Int. J. Psychophysiol. 18, 49–65.

Polich, J., 2007. Updating P300: an integrative theory of P3a and P3b. Clin. Neurophysiol. 118, 2128–2148.

Sabeti, M., Katebi, S., Boostani, R., 2009. Entropy and complexity measures for EEG signal classification of schizophrenic and control participants. Artif. Intell. Med. 47 (3), 263–274.

Sabeti, M., Moradi, E., Katebi, S.D., 2011. Analysis of neural sources of P300 event-related potential in normal and schizophrenic participants. Adv. Exp. Med. Biol. 696, 589–597.

Sanei, S., Chambers, J.A., 2007. EEG Signal Processing. John Wiley & Sons.

Schimpf, P.H., Liu, H., 2008. Localizing sources of the P300 using ICA, SSLOFO and latency mapping. J. Biomech. Biomed. Biophys. Eng. 2 (1), 1–11.

Spm8 (statistical parametric mapping) software, available at http://www.fil.ion.ucl.ac.uk/spm/software/spm8.

Stevens, A.A., Skudlarski, P., Gatenby, J.C., Gore, J.C., 2000. Event-related fMRI of auditory and visual oddball tasks. Magn. Reson. Imaging 18, 495–502.

Talairach, J., Tournoux, P., 1988. Co-planar Stereotaxic Atlas of the Human Brain. Thieme, Stuttgart, Germany.

Volpe, U., Mucci, A., Bucci, P., Merlotti, E., Galderisi, S., Maj, M., 2007. The cortical generators of P3a and P3b: A LORETA study. Brain Res. Bull. 73, 220–230.

Wong, D.D., Development of a Time-restricted Region-suppressed ER-SAM Beamformer and its Application to an Auditory Evoked Field Study. Master Thesis.